



RV Educational Institutions[®]
RV College of Engineering[®]

Autonomous
Institution Affiliated
to Visvesvaraya
Technological
University, Belagavi

Approved by AICTE,
New Delhi

Go, change the world

DEPARTMENT OF MECHANICAL ENGINEERING

Structural Mechanical Analysis Of External Gear Pump End Cover

PROJECT REPORT

Submitted by

ASHWIN SUDARSHAN

1RV18ME030

Under the guidance of

Dr. VL Jagannatha Guptha

Assistant Professor

Department of Mechanical Engineering

R V College of Engineering

Mr. Sudharsan Sriram

DC-MO/SEG-IN

Bosch Rexroth, Hejjala

**In partial fulfillment for the award of degree
of**

Bachelor of Engineering

in

Mechanical Engineering

2021-2022

RV COLLEGE OF ENGINEERING®, BENGALURU-59

(Autonomous Institution Affiliated to VTU, Belagavi)

DEPARTMENT OF MECHANICAL ENGINEERING



CERTIFICATE

This is to certify that the major project work titled '*Structural Mechanical Analysis Of External Gear Pump End Cover*' is carried out by **Ashwin Sudarshan (1RV18ME030)** who is a bonafide student of RV College of Engineering, Bengaluru, in partial fulfillment for the award of degree of **Bachelor of Engineering in Mechanical Engineering** of the Visvesvaraya Technological University, Belagavi during the year 2021-2022. It is certified that all corrections/suggestions indicated for the Internal Assessment have been incorporated in the major project report deposited in the departmental library. The major project report has been approved as it satisfies the academic requirements in respect of major Project Work (18MEP81) prescribed by the institution for the said degree.

Dr. VL Jagannatha Guptha

Dr. M KRISHNA

Dr. K N SUBRAMANYA

**Assistant Prof.
Dept. of Mechanical
Engineering**

**Prof. and Head
Dept. of Mechanical
Engineering**

**Principal
RV College of Engineering®
Bangalore**

External Viva

Name of Examiners

Signature with Date

1

2

INTERNSHIP CERTIFICATE

rexroth

A Bosch Company

Mivin Engg. Technologies (P) Ltd.
VSTPPL Compound, Survey No. 81 & 82/1,
Bengaluru-Mysuru Road,
Hejjala Village, Bidadi Hobli,
Ramanagara Dist. - 562 109 INDIA
Tel : +91 (0) 80 2301 2777
Tele Fax : +91 (0) 80 2301 2788
CIN : U2910KA2002PTC031230

Date: 19 July 2022

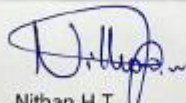
CERTIFICATE

This is to certify that **Mr. Ashwin Sudarshan, USN No: 1RV18ME030**, has undergone Bachelor of Engineering Internship between 18th April 2022 to 18th July 2022, in our organization on the topic of "**Structural Mechanical Analysis of External Gear Pump End Cover**".

During the above period, conduct of Mr. Ashwin Sudarshan has been Good.

Thanking you,

For MIVIN Engg. Technologies (P) Ltd



Nithan H T
Manager HR&IR

RV COLLEGE OF ENGINEERING®, BENGALURU-59

(Autonomous Institution Affiliated to VTU, Belagavi)

DEPARTMENT OF MECHANICAL ENGINEERING



DECLARATION

I, **Ashwin Sudarshan (1RV18ME030)** a student of Eighth Semester B.E, Mechanical Engineering, RV College of Engineering, Bengaluru hereby declare that the project titled **Structural Mechanical Analysis Of External Gear Pump End Cover** is carried out by me and submitted in partial fulfillment for the award of the Degree of Bachelor of Engineering in Mechanical Engineering for the academic year 2021-2022.

Further I declare that the content of the project report has not been submitted previously by anybody for the award of any degree or diploma to any other University.

I also declare that any Intellectual property rights generated out of this project carried out at Bosch Rexroth, Bangalore will be property of Bosch Rexroth, Bangalore and I will be only one of the co-authors of the same.

Place: Bengaluru

Date:

Name

Signature

1. Ashwin Sudarshan

(1RV18ME030)

ACKNOWLEDGEMENT

The successful completion of this project work was made possible through the valuable contribution of several people. To say thank you to all of them is not even enough to express our gratitude.

My first debt of gratitude and deep regards must go to our guides **Dr.VL Jagannatha Guptha**, Assistant Professor, Department of Mechanical Engineering and **Mr. Sudharsan Sriram**, DC-MO/SEG-IN, Bosch Rexroth, Hejjala for their valuable and inspiring guidance, wholehearted support, suggestions, patience and constant encouragement throughout my project work and immense help in the preparation of this thesis. The blessing, help and guidance given by them from time to time shall carry me a long way through my journey.

My sincere thanks to **Dr. Krishna M**, Professor and Head, Department of Mechanical Engineering, RVCE for his support and encouragement.

I express sincere gratitude to our beloved Principal, **Dr. K.N. Subramanya** for his appreciation towards this project work.

I thank all the **teaching staff and technical staff** of Mechanical Engineering department, RVCE for their help.

Lastly, I would like to thank my **Parents** for their unending support throughout the course of this project.

ABSTRACT

The global gear pumps market has been forecasted to arrive at 660.16 million USD by 2026, accelerating at a CAGR of 6.08 percent. Gear pumps perceive applications where accurate dosing or high-pressure output is required. But, the challenge of the work lies in the derivation of a suitable FE model, which captures the complex functionality of external gear pumps in operation and provides information about the stress distribution of the gear pump end cover. In this context, many researched works focused their attention on the development of the housing but very few or no work was focused on the optimization of end covers. The objective of this work was to develop a suitable FE model to evaluate static strength for future use, to avoid failures.

A base model was created from an existing solo housing model used at Rexroth. Another base model was created for a tandem housing model. The interactions and loading conditions were compared for both and the right values were found. The gear calculations were carried out for the model, the surface was partitioned and the boundary conditions, loading conditions and constraints were finalized. Then, the values of maximum principal stress in MPa and deformation in mm were observed for the same. Five iterations were carried out using the base model as reference. These iterations had different types of meshing, each one finer than the other. Tetrahedral meshing was used for most of the iterations.

Values of maximum principal stress and deformation were observed for each of the iterations. It was found that the maximum principal stress varied slightly between the base model and the five iterations. Out of the five iterations, the 4th iteration had a value of 243 MPa and thus it was shortlisted for future use. It was also observed that the deformation was almost the same for all 5 iterations i.e. 0.1138 mm and very close to the base model i.e. 0.1137 mm. Another important observation that was made was that the maximum principal stress was perpendicular to the direction of the crack. This was proven by performing a burst pressure test, where the end cover failed at 400 bar. The outcome of the project was to optimize the end cover model which failed at a pressure of 350 bar, to avoid such instances in the future. It is also possible to perform further optimization by defining strain as a parameter and using strain gauge for accurate measurement of strains. Further, the thickness of end covers can be changed and then a stress assessment can be done for the same.

TABLE OF CONTENTS

ACKNOWLEDGEMENT	i
ABSTRACT.....	ii
TABLE OF CONTENTS.....	iii
LIST OF FIGURES	v
LIST OF TABLES.....	vi
LIST OF ACRONYMS	vi
CHAPTER 1	1
INTRODUCTION	1
1.1 Market Survey and Society Relevance.....	1
1.2 Literature Review	2
1.3 Research Gap.....	4
1.4 Objectives	5
1.5 Organization of the report.....	5
CHAPTER 2	6
THEORY AND CONCEPTS	6
2.1 External Gear Pump	6
2.2 Components of external gear pump.....	7
2.3 Construction or assembly of external gear pump.....	8
2.4 Working principle of external gear pump.....	9
CHAPTER 3	11
PROJECT METHODOLOGY.....	11
3.1 Problem Definition	11
3.2 Project Methodology.....	11
CHAPTER 4	13
GEAR CALCULATIONS	13
4.1 Calculation of Gear Forces	13
4.2 Resultant Gear Forces	14
4.3 Observations from gear calculations	15
CHAPTER 5	16
COMPARSION BETWEEN SOLO AND TANDEM HOUSING PUMPS.....	16
5.1 Solo Housing Pump.....	16
5.1.1 Interactions – Housing and End Cover	16

5.1.2 Interactions – Bushing and End Cover	17
5.1.3 Constraints	17
5.1.4 Loads - Pressure.....	18
5.1.5 Loads – Pre-stresses.....	19
5.2 Tandem Housing Pump	20
5.2.1 Interactions – Housing and End Cover	20
5.2.2 Constraints	20
5.2.3 Loads – Pressure.....	21
5.2.4 Loads – Pre-stresses.....	22
CHAPTER 6	23
RESULTS AND ANALYSIS.....	23
6.1 Base model.....	23
6.1.1 Maximum Principal Stress.....	23
6.1.2 Deformation.....	24
6.2 Iteration #1 (81888 elements).....	24
6.2.1 Maximum Principal Stress.....	25
6.2.2 Deformation.....	26
6.3 Iteration #2 (170466 elements).....	26
6.3.1 Maximum Principal Stress.....	27
6.4 Iteration #3 (244412 elements).....	27
6.4.1 Maximum Principal Stress.....	28
6.5 Iteration #4 (349758 elements).....	28
6.5.1 Maximum Principal Stress.....	29
6.6 Iteration #5 (576637 elements).....	29
6.6.1 Maximum Principal Stress.....	30
CHAPTER 7	32
CONCLUSION AND FUTURE SCOPE	32
7.1 Conclusion.....	32
7.2 Future Scope.....	32
REFERENCES	33

LIST OF FIGURES

CHAPTER 1

Fig 1. 1 Global Hydraulic Gear Pump Market.....	1
Fig 1. 2: End cover cracked at a pressure of 400 bar	4

CHAPTER 2

Fig 2. 1: Construction of an external gear pump	7
Fig 2. 2: Assembly of external gear pump	9
Fig 2. 3: Fluid transport in an external gear pump	10

CHAPTER 3

Fig 3. 1: Methodology.....	11
----------------------------	----

CHAPTER 4

Fig 4. 1: Distribution of pressure around gears.....	13
Fig 4. 2: Resultant Gear Forces.....	15

CHAPTER 5

Fig 5. 1: Interaction between housing and end cover	16
Fig 5. 2: Interaction between bushing and end cover	17
Fig 5. 3: All four bolts are constrained on the end cover.....	17
Fig 5. 4: Pressure of 230 bar acting on the end cover.....	18
Fig 5. 5: Pre-stresses of bolts.	19
Fig 5. 6: Housing and end cover interaction	20
Fig 5. 7: All four bolts are constrained on the end cover.....	21
Fig 5. 8: Pressure of 250 bar on the end cover.....	21
Fig 5. 9: Pre-stress for all four bolts on the end cover	22

CHAPTER 6

Fig 6. 1: Maximum Principal Stress for the base model.....	23
Fig 6. 2: Deformation for base model.....	24
Fig 6. 3: Maximum Principal Stress- Iteration #1.....	25
Fig 6. 4: Deformation – Iteration #1	26
Fig 6. 5: Maximum Principal Stress- Iteration #2.....	27

Fig 6. 6: Maximum Principal Stress- Iteration #3.....28

Fig 6. 7: Maximum Principal Stress- Iteration #4.....29

Fig 6. 8: Maximum Principal Stress- Iteration #5.....30

LIST OF TABLES

Table 6. 1: Summary of results obtained during the iterations31

LIST OF ACRONYMS

SHORT FORM OF ACRONYM	ACRONYM
CAGR	Compound annual growth rate
FEA	Finite Element Analysis
CAD	Computer Aided Drawing

CHAPTER 1

INTRODUCTION

1.1 Market Survey and Society Relevance

The global hydraulic pump market size is valued at USD 1.89 Billion in 2022 and is projected to reach USD 2.54 Billion by 2030. The gear pump market share is expected to increase by USD 660.16 million from 2021 to 2026, and the market's growth momentum will accelerate at a CAGR of 6.08%. Rexroth employs over 31,000 people worldwide and achieved total revenue of 6.2 billion euro in 2019.

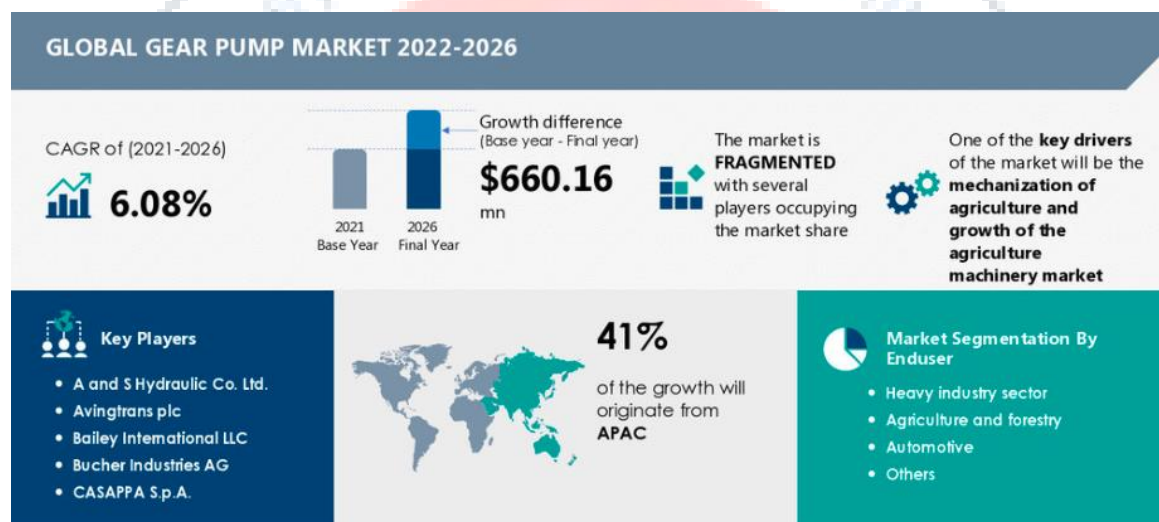


Fig 1. 1 Global Hydraulic Gear Pump Market

Fig 1.1 shows the global hydraulic gear pump market from 2022 to 2026. It shows the growth that will take place in the five year range. It shows that 41 percent of the growth will originate in the Asia Pacific region. It shows a 660 million USD increase in the growth between 2021 and 2026.

To remain competitive in the long term, it is necessary to shorten development times and optimize all structural components of pumps. To achieve these goals without complex and cost-intensive test series and to be able to react flexibly to customer requirements, it is necessary to calculate the fatigue of pump end covers. therefore, all test series for

evaluating and optimizing the pump end cover will be accompanied by a standardized method for fatigue analyses of the pump end cover (In the long run to reduce the number of fatigue tests). The challenge of the work lies in the derivation of a suitable FE model, which captures the complex functionality of external gear pumps in operation and provides information about the stress distribution of the gear pump end cover. In the future, the developed methodology should provide a reliable, computational proof of the fatigue strength of the pump end cover and thus minimize complex test runs with prototypes. During execution of the project, there was continuous exposure to CAD software like Creo and FEA tools like Abaqus

1.2 Literature Review

Gear pumps are a type of hydraulic pumps. High pressure gear pumps are chosen when such properties as hydraulic power transfer, basic construction, high capacity, cheapness, and easy assembling are required.

Today, as technological development and competition in the industry increase, the working system design is not good enough. The key point of the design is making the best. This means that the designed system should be cheaper and more effective. This can be achieved by optimum system designing and solving the formulation of an optimization problem. An optimization problem searches for the best solution and is characterized by a mathematical function that has a minimum and a maximum value for given boundary conditions.

E. Mucchi, et al. studied simulation of the running external gear pumps. They have modified their old models and created a new model. Authors then prepared a mathematical model and made dynamic simulations. The mathematical model was verified by an experimental study. At the end of the study authors obtained a reduction of 16% of the running in time [1].

W. Kollek and U. Radziwanowska studied micro pump body mass optimization. They have carried out a static analysis of the body of the micro pump. After analysis of stress and displacement distribution in the pump body, a mass optimization of construction was made. The optimized micro pump body has resulted in more than 30% increase in

energetic efficiency, compared to the original pump [2].

W. Fiebig and M. Korzyb, developed a mathematical model for studying vibration and dynamic loads in external gear pumps. Calculations have been carried out using MATLAB/Simulink software. The influence of pressure and rotational speed on the dynamic forces in the bearings has been analyzed [3].

P. Osiński et al. studied optimization of volume efficiency of a hydraulic external gear pump after tooth root undercutting. They have carried out several experimental tests for varied number of revolutions. They measured mechanical and volumetric efficiency, mechanical and hydraulic power, moment of losses [4].

H. Shen et al. have carried out a computational fluid dynamic analysis to analyze pressure distribution of internal flow field of the gear pump and constructed the unidirectional flow-solid coupling model of a gear, to acquire the contact stress of tooth surface, using Ansys workbench software [5].

P. Casoli et al. have carried out an optimization study of an external gear pump. They used a software developed by the University of Parma for analysis and optimization of gear pumps. The procedure is based on a path search method, known as steepest descent, which optimizes the considered parameters, starting from a design, taken as the initial reference. The objective functions, defined for the optimization, permit to account for the volumetric efficiency, the delivery pressure ripple and the maximum and minimum pressure peaks during the meshing process [6].

S. Wang et al. studied the instantaneous pressure of the meshing action in the external gear pumps and motors. The study employed the optimization theorem to analyze the nonlinear dynamical equations, to define the instantaneous flow area, overlapped by the wear-plate profiles and control volumes [7].

Noorpoor created a model and simulation of a diesel engine gear oil pump and utilised a solver to do a fluid flow study. The pump's redesign and optimization have been addressed, and the results have been contrasted with experimental and earlier findings. The method employed in this case involved employing dynamic meshes to investigate the flow across a set number of time steps separated by a

tooth rotating cycle [8].

1.3 Research Gap

In the literature review done, a standardized method for optimization of end covers was missing. Hence, we are going in depth regarding end covers and developing a standard model for future use to avoid failures as shown in the figures below. The pump cover will be designed first and a static structural analysis will be performed. Then an optimization will be carried out, using the results of the static analysis, and several iterations will be obtained. Finally, the best of the iterations will be chosen as the final design.



Fig 1. 2: End cover cracked at a pressure of 400 bar

Fig 1.2 shows the existing model at Rexroth getting cracked at a pressure of 400 bar. A burst pressure test was carried out wherein it was observed that the direction of the crack was perpendicular to the direction of maximum principal stress. The same was also proved numerically.

1.4 Objectives

- The stress distribution for the end cover must be found out and the critical areas where failure is most likely must be the main area of focus.
- The magnitude of Maximum Principal stress & deformation /displacement should be computed as well and to identify the few critical points & noted.
- Optimal FE model fidelity regarding the results quality and computational time is required for stress assessment of the gear pump end cover
- Motivation is to improve the strength of the end covers which will be helpful for further material optimization.

1.5 Organization of the report

Chapter 1: INTRODUCTION: gives a brief introduction about the market survey, problem definition followed by literature review and organization of report.

Chapter 2: THEORY AND CONCEPTS: gives a brief overview on basics of external gear pumps.

Chapter 3: PROJECT METHODOLOGY: defines the problem statement of this work, along with the methodology of work.

Chapter 4: GEAR CALCULATIONS: explains the gear force calculations that have been done as part of modelling of the end cover.

Chapter 5: COMPARISON BETWEEN SOLO AND TANDEM HOUSING PUMPS: gives an overview of the difference in loading conditions and interactions between solo and tandem housing pumps.

Chapter 6: RESULTS AND ANALYSIS: brings out detailed analysis of the gear pump end cover base model along with its iterations.

Chapter 7: CONCLUSION AND FUTURE SCOPE: Presents conclusions of the project work and presents concepts for future work which can be carried out.

CHAPTER 2

THEORY AND CONCEPTS

2.1 External Gear Pump

An external gear pump converts the mechanical energy (torque and speed) into hydraulic energy (flow and pressure). It is a rotary positive displacement type of pump. External gear pumps are available with spur, helical, and herringbone gears in single or double (two sets of gears) pump arrangements. Large-capacity external gear pumps typically use helical or herringbone gears, as the noise emission is lesser because the pressure rise does not take place suddenly. A demerit of helical teeth is the emergence of the axial force. A lower noise level without additional axial force is achievable in gear pumps with double helical teeth, but extensive production technology must be employed [20].

Small external gear pumps typically operate at 1750 or 3450 rpm, while larger models operate at speeds up to 640 rpm. External gear pumps have tight tolerances and shaft supports on both sides of the gear. This allows operation at pressures above 3,000 psi / 200 bar, making it ideal for hydraulic applications. With four bearings in the liquid and tight tolerances, they are not well suited to handling abrasive or extreme high temperature applications [17]. because of the reversible redox processes. Numerous industries connected to energy storage have used pseudo capacitors. The performance of a supercapacitor as a whole is significantly influenced by the electrode materials. External gear units are also popular for precise transfer and metering applications involving polymers, fuels, and chemical additives. Some of the advantages of external gear pump are its high speed, high pressure, relatively quiet operation and no overhung bearing loads and combination of several pumps are possible. The disadvantages of an external gear pump are fixed displacement of the fluid, high pulsation greater than the internal gear pumps or vane pumps and lesser than the axial piston pump, no solids are allowed as it would create physical wear of the internal components causing reduced output or complete damage to the pump [27]. Some of the common applications of external gear pump are forklift, tractors, construction and agricultural machineries.

2.2 Components of external gear pump

The entire pump comprises of only a few components, which leads to a high degree of functional integration. Therefore, all the load-carrying components must fulfil additional tasks to ensure the functionality of the pump.

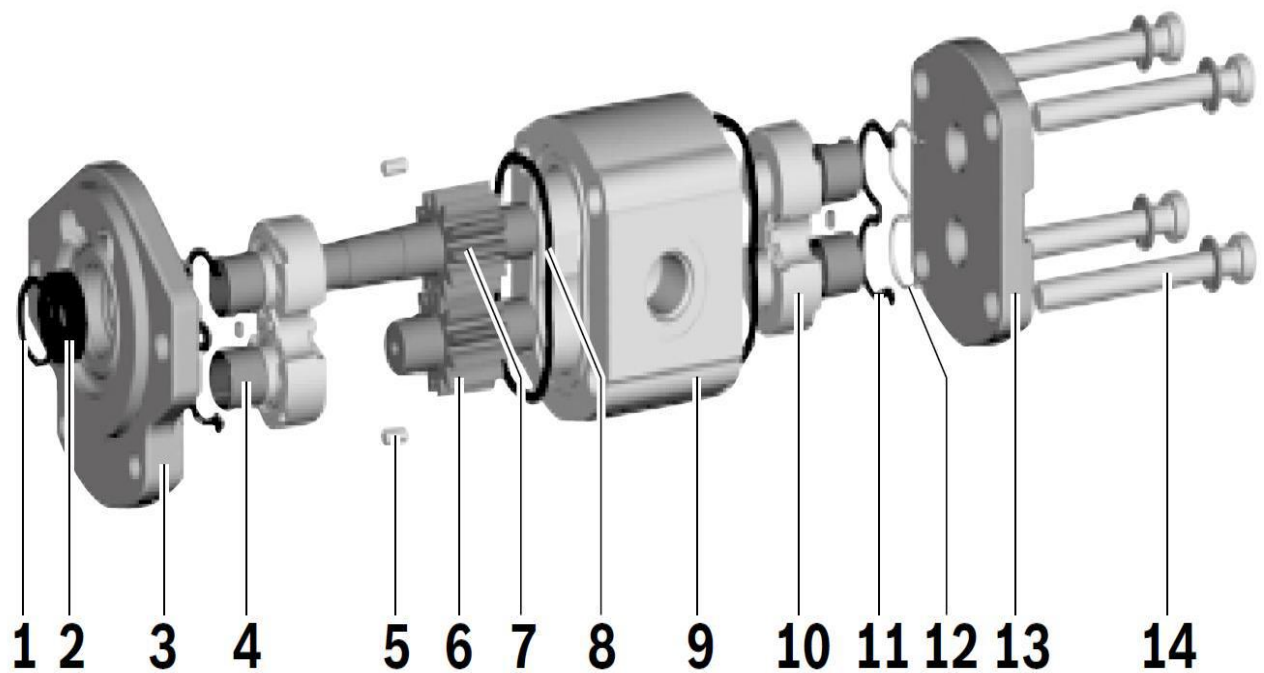


Fig 2. 1: Construction of an external gear pump

- | | |
|------------------|-----------------------|
| 1 Snap ring | 8 Housing seal ring |
| 2 Shaft seal | 9 Pump housing |
| 3 Front cover | 10 Bearing bushing |
| 4 Slide bearings | 11 Axial field seal |
| 5 Centering pin | 12 Supporting element |
| 6 Gear wheel | 13 End Cover |
| 7 Drive shaft | 14 Torque screws |

Fig 2.1 shows the construction of an external gear pump and its components which include the front cover made of Aluminum, the housing which is also made of Aluminum. It also comprises of the end cover which is made up of grey cast iron i.e. EN-GJL-250

2.3 Construction or assembly of external gear pump.

The housing, front and end covers, and two spur gear wheels supported by bearing bushes make up the particular external gear pump. The shaft seal ring typically seals the drive shaft, which protrudes from the front cover. Shafts that are supported by journal/slide bearings support the gears on both sides. The sliding bearings withstand bearing forces. These sliding bearings offer excellent dry-running characteristics and are especially well suited for high pressures and slow shaft rotational speeds. Both gear wheels feature 12 teeth and are entirely similar to one another [19].

As shown in Fig 2.2, the internal sealing of the pressure chambers is achieved by operating pressure-dependent forces. This ensures optimum efficiency of the gear pump. On the outer face, the movable bearing bushes are pressurized with the operating pressure and pressed as seals against the gear wheels. This pressure also includes the pressure exerted from seals and hence is slightly higher than the pressure on the inner face of bushing towards gears. If the pressure difference is large, it would create wear on the gear and bushing side faces and obstructing the rotation of the shaft leading to reduced efficiency of the pump. In addition, special axial field seals form the boundary of the pressurized zone. The radial sealing at the tips of the gear teeth against the pump housing is provided by smallest possible gaps that are formed pressure-dependent between the gear wheels and the housing [19].

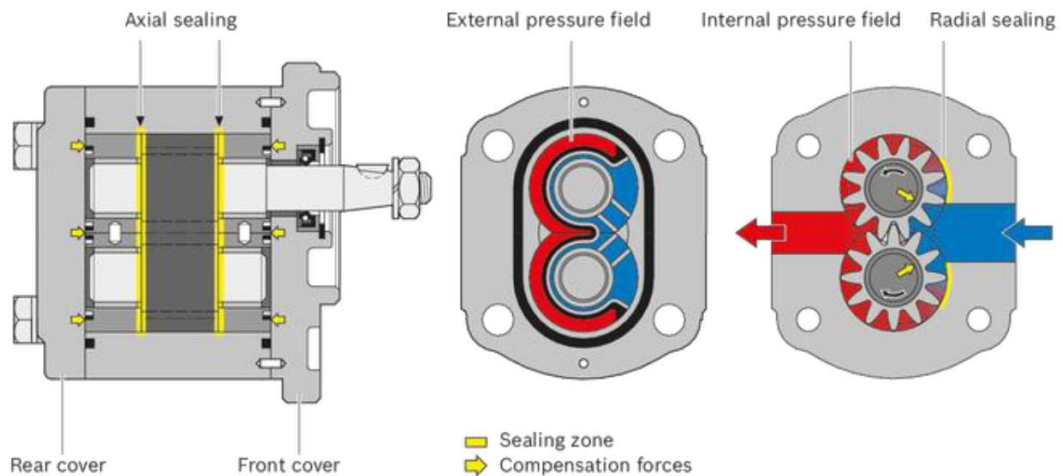


Fig 2. 2: Assembly of external gear pump[11]

2.4 Working principle of external gear pump

During operation the inlet side of the pump has the suction pressure and the delivery side of the pump has the high operating pressure. The pressure of the fluid must increase proportionally from the suction port into the first tooth space volume until it reaches a maximum operating pressure at the delivery port of the gear pump. Due to this increase in pressure developed during operation, the gear pump would experience radial loads proportional to the pressure from suction side to the delivery side. The fluid transfer in external gear pump takes place by the meshing of gears caused by the rotation of driving and driven shafts [14].

Fig 2.3 shows the different stages during the fluid transport. The process starts when the low- pressure fluid enters the gear pump at the suction port. The unmeshing of the driving and driven gears at the inlet region creates an expanding volume, which forces the low-pressure fluid to fill the empty region at the inlet of the pump. The low-pressure fluid occupies the chamber formed between the gear teeth faces and is trapped between the interior of the housing and gear faces with the rotation of the shaft. As the gears rotate, the gear faces impart energy to the carrying fluid. The trapped fluid travels along the circumference of the interior of housing and reaches the discharge side of the gear pump. Finally, when the meshing of gears takes place in the high-pressure region, the fluid in the

chambers of the meshed teeth is forced out of the chamber causing it to leave the gear pump through the discharge port under high pressure [25].

The volume flow rate of the pump is directly dependent on the volume of each chamber carrying the fluid. In addition, if the clearance between the interior of casing and the top land of gear teeth is large, then the fluid might flow back to the low-pressure region of the pump leading to reduced efficiency. Hence, an optimal design with the right balance between the number of gear teeth and the clearance between housing and top land of gear teeth is therefore necessary. There are 12 teeth on each gear in the high-pressure gear pump model considered in this thesis and this keeps both the flow pulsation and noise emission to a minimum as possible [7].

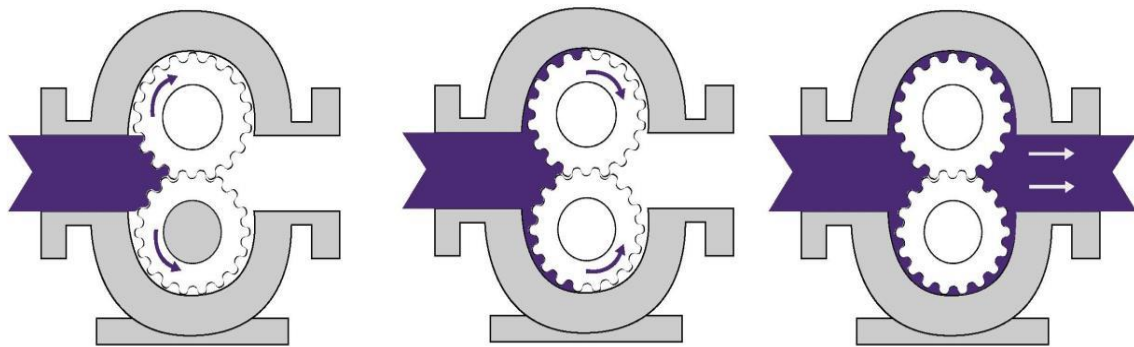


Fig 2. 3: Fluid transport in an external gear pump[14]

CHAPTER 3

PROJECT METHODOLOGY

3.1 Problem Definition

The challenge of the work lies in the derivation of a suitable FE model, which captures the complex functionality of external gear pumps in operation and provides information about the stress distribution of the gear pump end cover

3.2 Project Methodology

The Fig 3.1 describes the methodology followed for completing the project work.

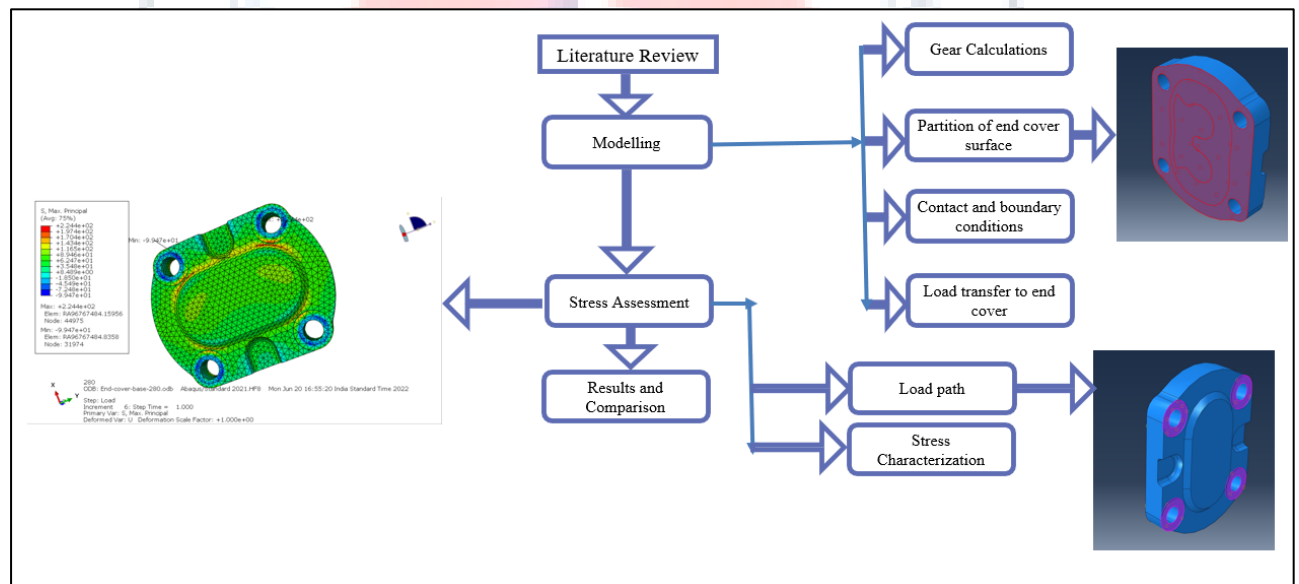


Fig 3. 1: Methodology

- Once the literature review is done with, after collecting sufficient data, we proceed with the modelling of the end cover
- The most important aspect of modelling is the gear calculations which has been explained in the upcoming chapter.
- Partitioning of the end cover surface is done so as to improve the meshing and according to the requirement of various iterations carried out.
- Once the partitioning is done, contact and boundary conditions are determined, and

inputs are given in the ABAQUS CAE Software

- Once we have determined all the necessary boundary conditions, we proceed with the stress assessment where we look at 2 important factors- Maximum Principal Stress and Deformation.
- Once we obtain all these values, we can compile the results and make observations.



CHAPTER 4

GEAR CALCULATIONS

4.1 Calculation of Gear Forces

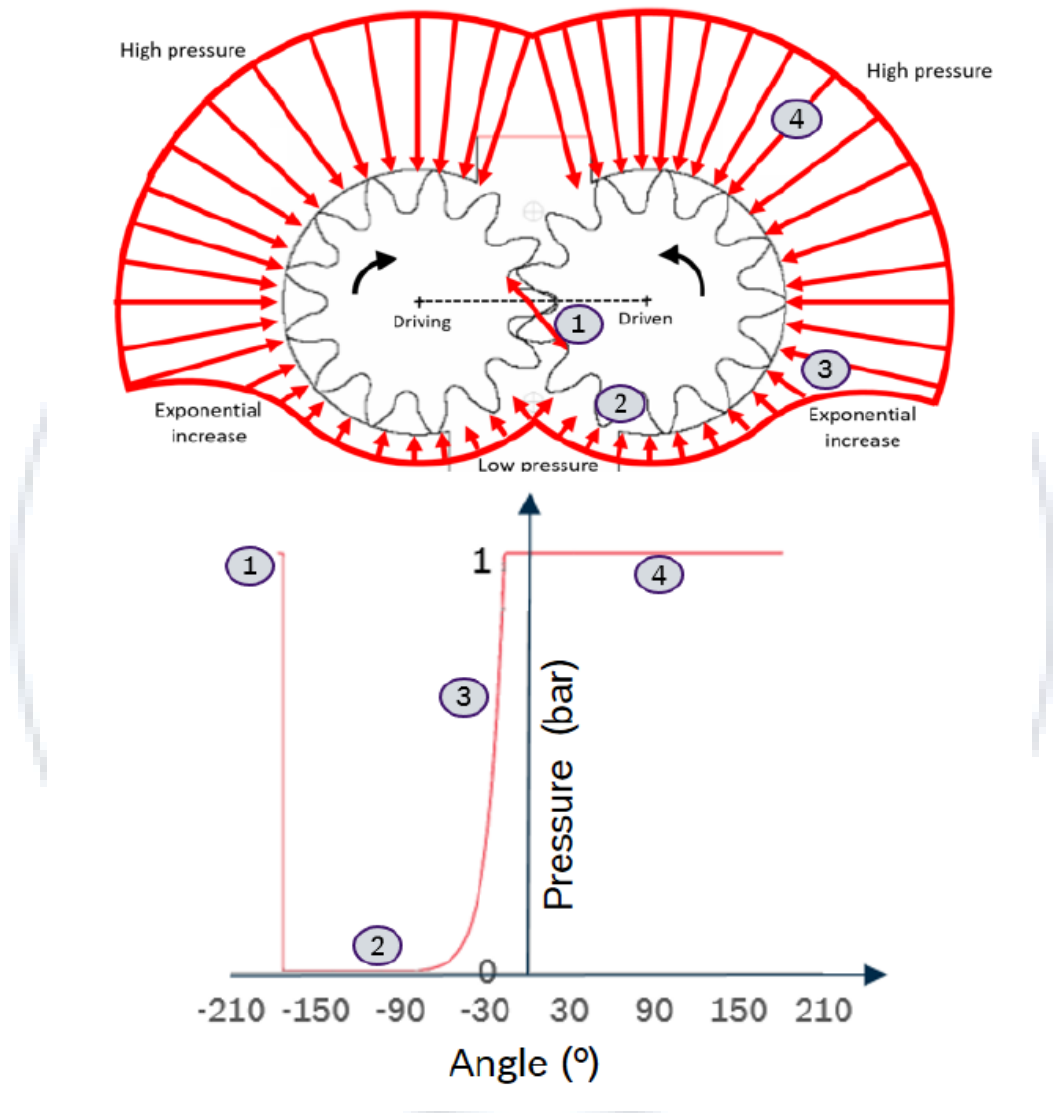


Fig 4. 1: Distribution of pressure around gears

Fig 4.1 gives the following observations -

- There are 12 teeth on both driving and driven gears.
- The forces considered are the forces resulting from the transient pressure

distribution and the meshing force of the teeth resulting from the torque transmitted by the two gears.

- The region 1 on the gear and pressure distribution graph shows the one-half of the gear teeth of the driving gear below the horizontal axis under high pressure and below this the gear teeth is in contact and hence the pressure drops down to suction pressure as shown in region 2.
- The part of the gear in region 2 is completely under suction pressure and the part of the gear in region 4 is under high pressure and in between in the region 3 the pressure changes from suction pressure to high pressure exponentially on the driven gear.

4.2 Resultant Gear Forces

The Gear forces are calculated using a Mathcad Tool available at Bosch Rexroth.

The resultant direction of the gear forces is as shown in the Fig 4.2. In the current position of the gears, the angle of resultant gear force on driving gear is slightly higher than the driven gear because of the position of the gear teeth in the current position the high-pressure starts slightly later on the driven gear. In addition, the magnitude of the resultant force on driving gear is smaller than the driven gear as the teeth meshing force acts opposite to the direction of resultant force, which causes the reduction in the amplitude of resultant force on driving gear. The x-component of both the resultant forces of both the gears are 9016 N equal in magnitude and opposite in direction. The y-component of resultant force on driving and driven gear are -19000 N and -12002 N respectively. In addition, the angles Θ_1 and Θ_2 are 27° and 22° respectively.

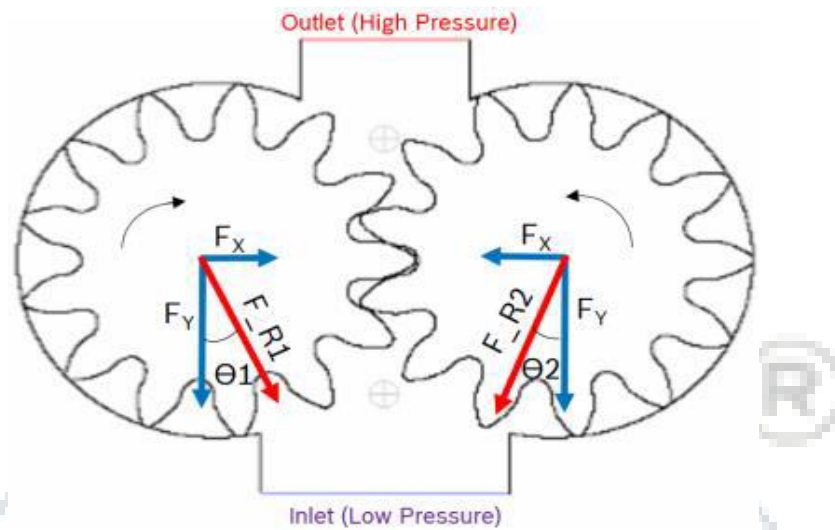


Fig 4. 2: Resultant Gear Forces

4.3 Observations from gear calculations

- Since the x-component of the resultant gear forces are equal in magnitude and opposite in direction it is assumed that this force only helps to keep the split bushings together and does not transmit any load to the end cover and only the y-component of the resultant forces are transmitted to the end cover.
- Hence, a simulation is performed to check the variation of the stresses on the housing for the two loading conditions, one with both x and y-components of the resultant forces are applied in the finite element modelling and the other with only the y-component.
- It is found that both the x component forces cancel out each other, so we have taken into consideration only the y component forces.

CHAPTER 5

COMPARISON BETWEEN SOLO AND TANDEM HOUSING PUMPS

5.1 Solo Housing Pump

5.1.1 Interactions – Housing and End Cover

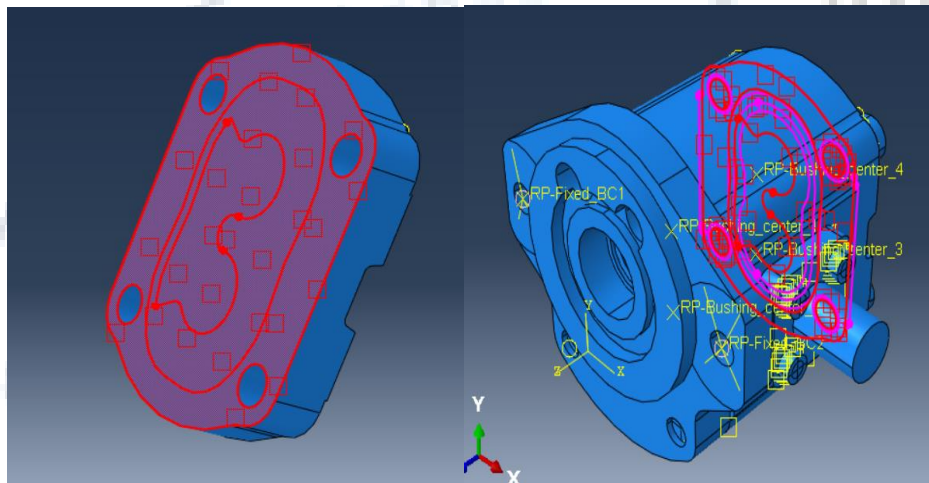


Fig 5. 1: Interaction between housing and end cover

Fig 5.1 shows the interaction of the end cover with the housing surface. This is also known as the initial step in the model. The surface is partitioned accordingly and the interaction can be observed. This interaction is mainly due to the contact between the end cover and the housing.

5.1.2 Interactions – Bushing and End Cover

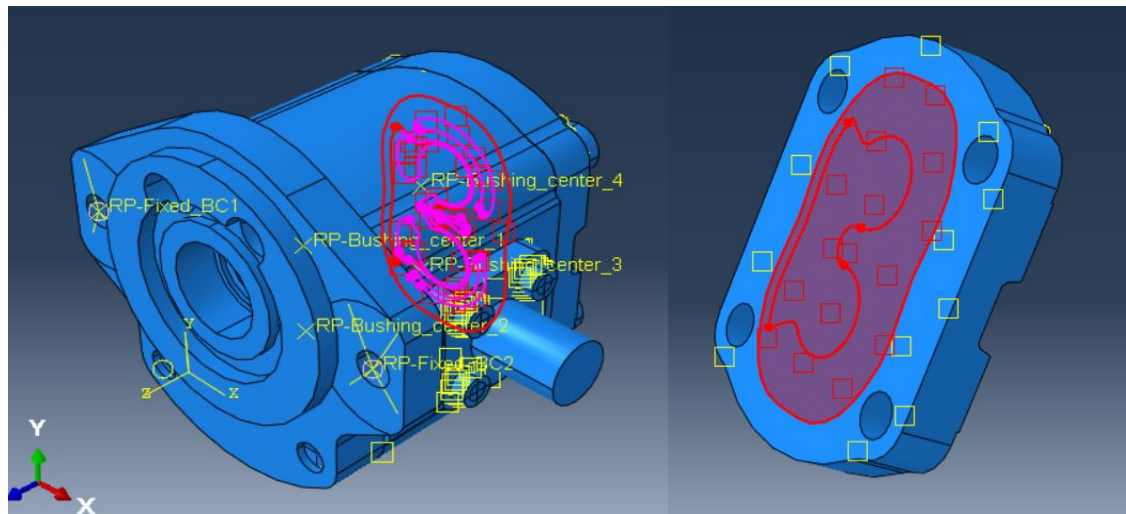


Fig 5. 2: Interaction between bushing and end cover

Fig 5.2 shows the interaction of the end cover with the bushing surface. This is also included in the initial step of the model. The interaction between bushing and end cover takes place only in solo housing pumps and not the tandem housing pumps.

5.1.3 Constraints

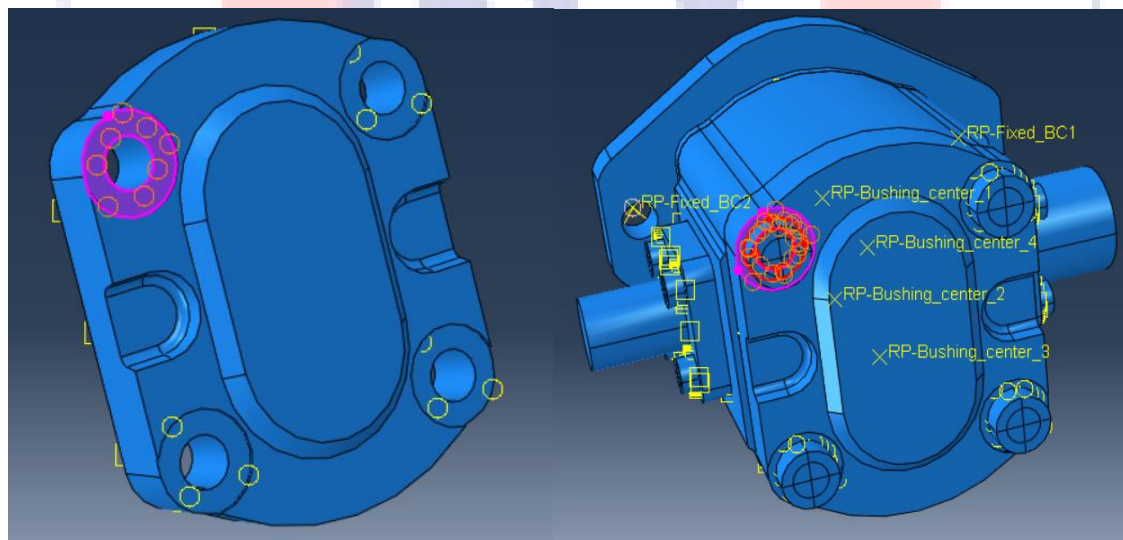


Fig 5. 3: All four bolts are constrained on the end cover

Fig 5.3 shows all the four bolts on the end covers being constrained. All 4 bolts are of M12 diameter. There is a 1 mm chamfer on each of the bolts. These bolts have pre-

stresses of 26000N. The bolts are highlighted as shown in orange in the right hand side of the figure.

5.1.4 Loads - Pressure

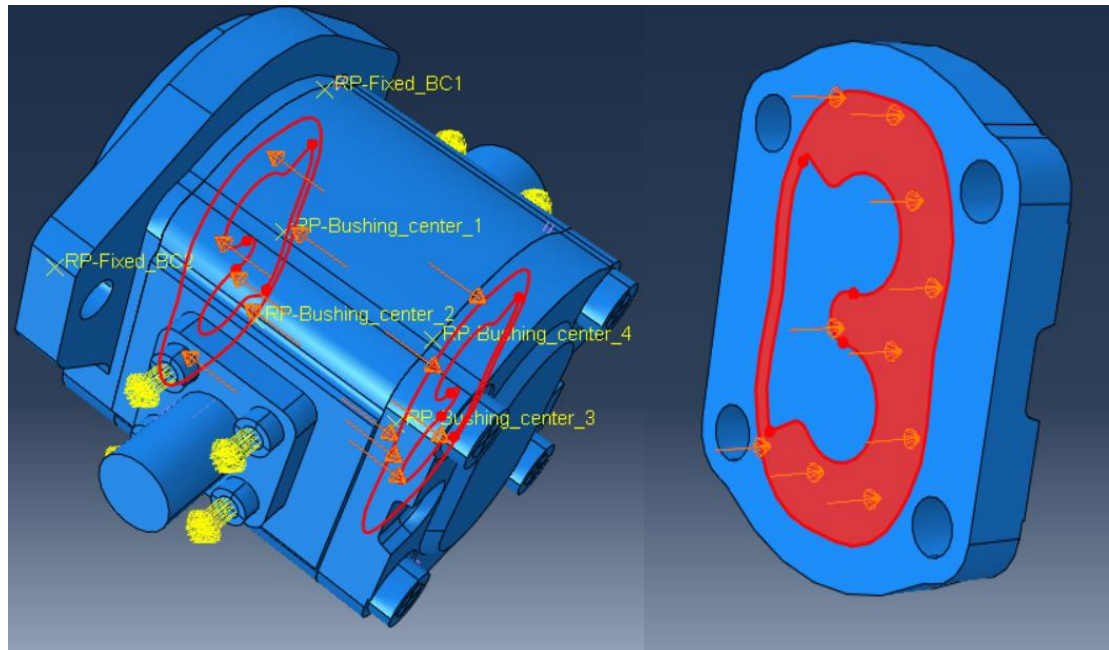


Fig 5. 4: Pressure of 230 bar acting on the end cover

Fig 5.4 shows a pressure of 230 bar acting on the end cover surface. The required boundary conditions have been applied perpendicularly as shown above in the right side of the figure. The pressure has been applied in the red area shown perpendicular to the surface.

5.1.5 Loads – Pre-stresses

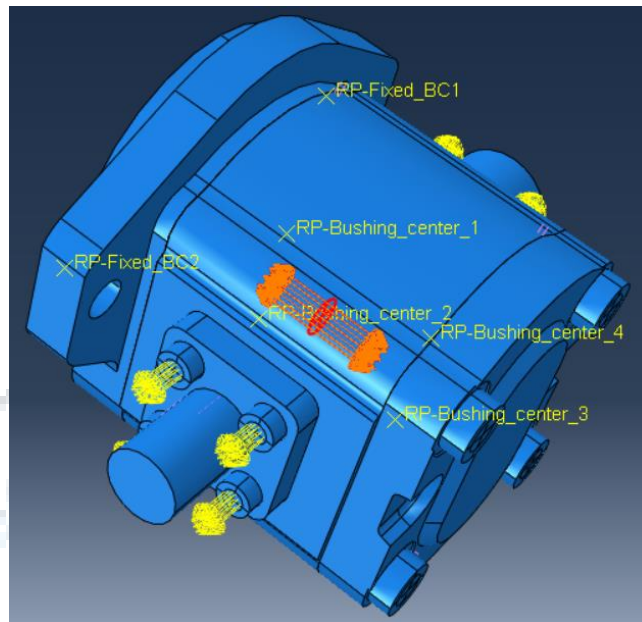


Fig 5. 5: Pre-stresses of bolts.

Fig 5.5 shows the pre-stresses of bolts acting for all four bolts. A load of 26000N is observed in the orange highlighted part of the figure. It is part of the necessary boundary conditions which have been specified and determined after ample comparison with solo and tandem housing pumps.

5.2 Tandem Housing Pump

5.2.1 Interactions – Housing and End Cover

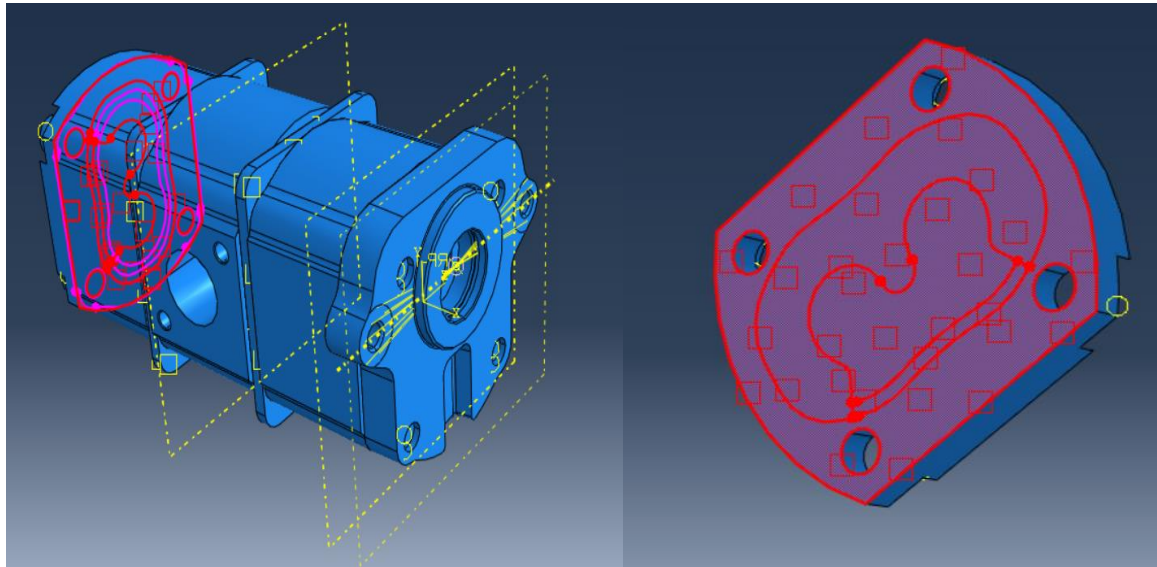


Fig 5. 6: Housing and end cover interaction

Fig 5.6 shows the interaction of the housing and the end cover for the tandem housing pump. There is no interaction between the bushings and the end cover for tandem housing pump unlike solo housing pump. It can be observed in the red part in the right hand side of the image.

5.2.2 Constraints

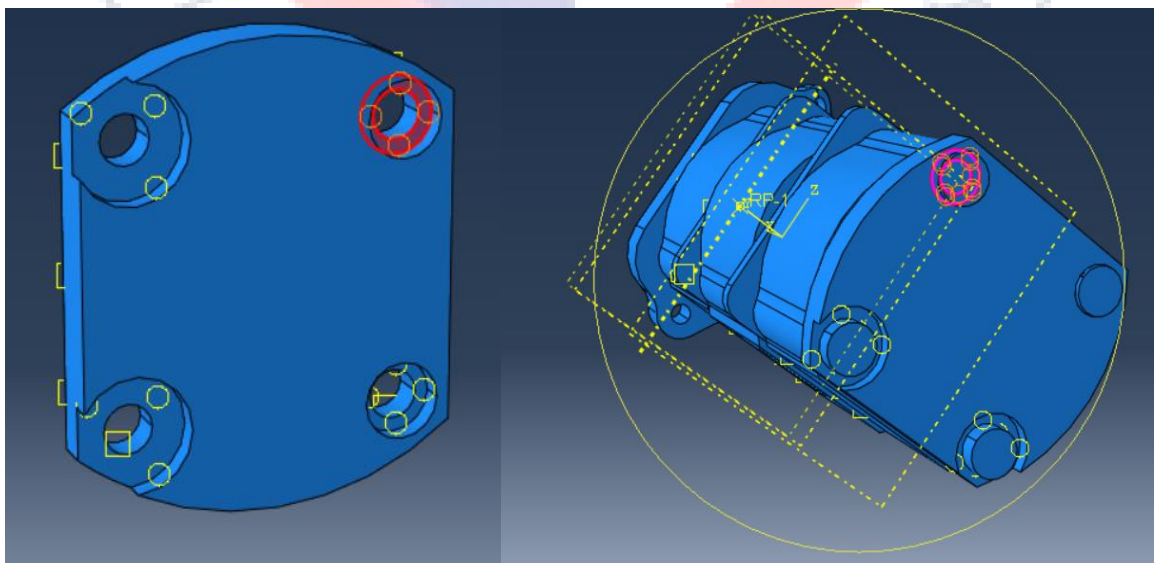


Fig 5. 7: All four bolts are constrained on the end cover

Fig 5.7 shows all four bolts on the end cover constrained, similar to solo housing pump. After sufficient comparisons between tandem and solo housing pumps it has been observed that the necessary boundary conditions include certain constraints that have to be applied as shown in the highlighted part of the figure.

5.2.3 Loads – Pressure

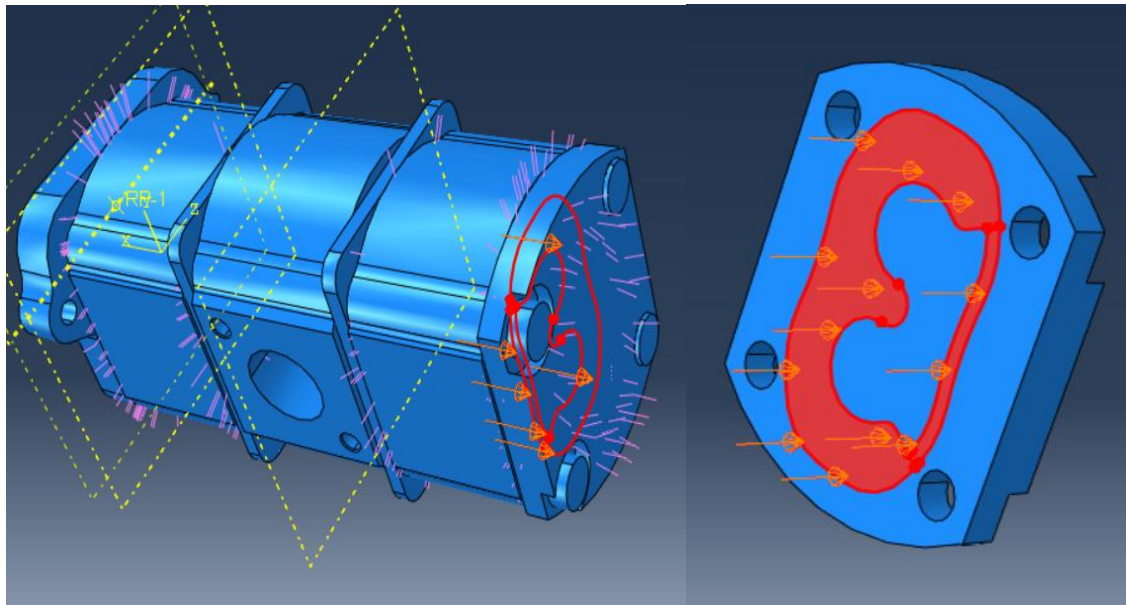


Fig 5. 8: Pressure of 250 bar on the end cover

Fig 5.8 shows a pressure of 250 bar acting on the end cover due to the tandem housing. It can be observed in the right part of the figure highlighted in red that the pressure load is acting in a perpendicular direction. It is part of the necessary boundary conditions which were derived from initial comparisons.

5.2.4 Loads – Pre-stresses

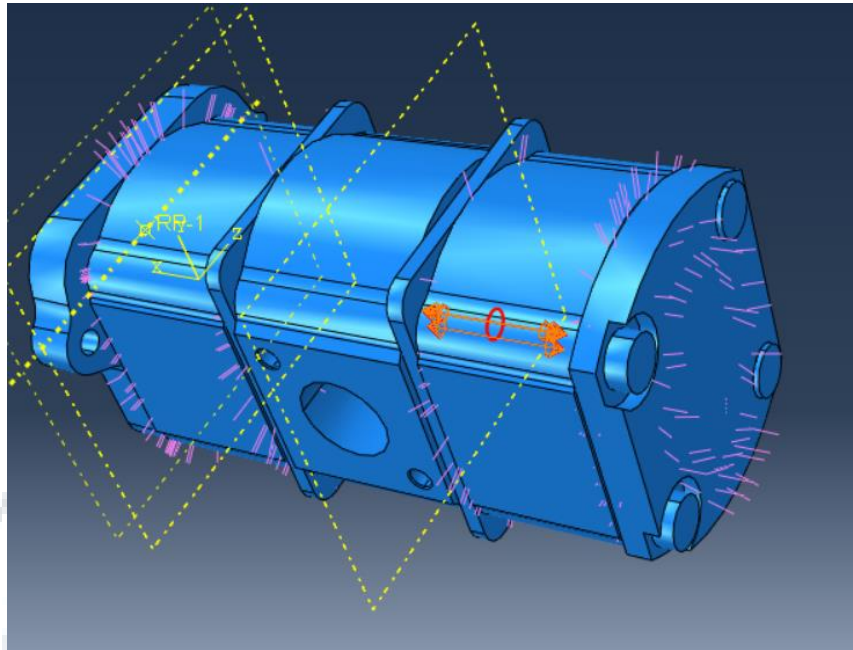


Fig 5. 9: Pre-stress for all four bolts on the end cover

Fig 5.9 shows a Pretension of 26000 N for all 4 bolts on the end cover. It is part of the necessary boundary conditions that are required. These bolts are of M12 Diameter and the pre stresses produced by them amount to 26000N for all the four bolts. It is highlighted in red in the figure.

CHAPTER 6

RESULTS AND ANALYSIS

6.1 Base model

The base model was first submitted for analysis and results were obtained. These results were used as a benchmark for further iterations carried out. The end cover is made of EN-GJL-250 Cast iron, which is a brittle material, having a yield strength of 250MPa. It is a form of grey cast iron. 2 important parameters were observed- Maximum Principal Stress and Deformation

6.1.1 Maximum Principal Stress

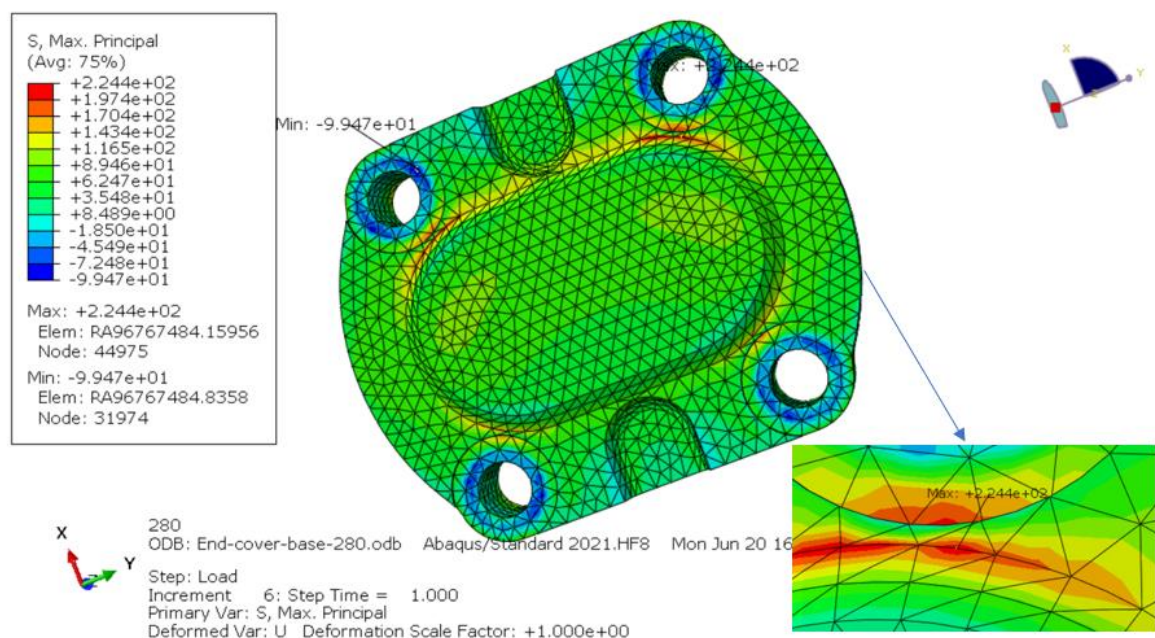


Fig 6. 1: Maximum Principal Stress for the base model

Fig 6.1 shows a Maximum Principal Stress of 224MPa for the base model. It is observed that the maximum principal stress is perpendicular to the direction of the crack. The stress is observed to be highest in the region where the cover is likely to fail most easily i.e. the joint in the discharge side of the end cover.

6.1.2 Deformation

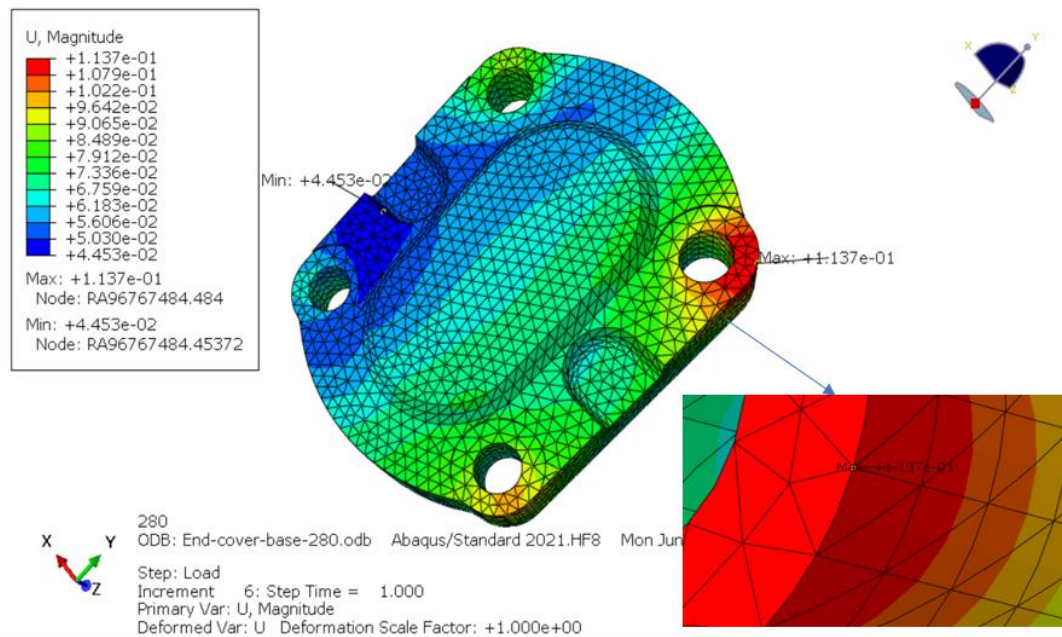


Fig 6. 2: Deformation for base model

Fig 6.2 shows a deformation of 0.1137mm for the base model. It can be observed that the maximum deformation is in the suction side of the end cover and it can also be seen that the maximum value of deformation is due to the sliding of the end cover i.e. an upward motion that takes place. It was expected that there would be a symmetrical deformation pattern but due to the siding of the cover, the suction side shows maximum deformation.

6.2 Iteration #1 (81888 elements)

Iteration #1 consists of a fine mesh, with the number of elements being increased from 33674 in the base model to 81888 elements. The results are put together as follows-

6.2.1 Maximum Principal Stress

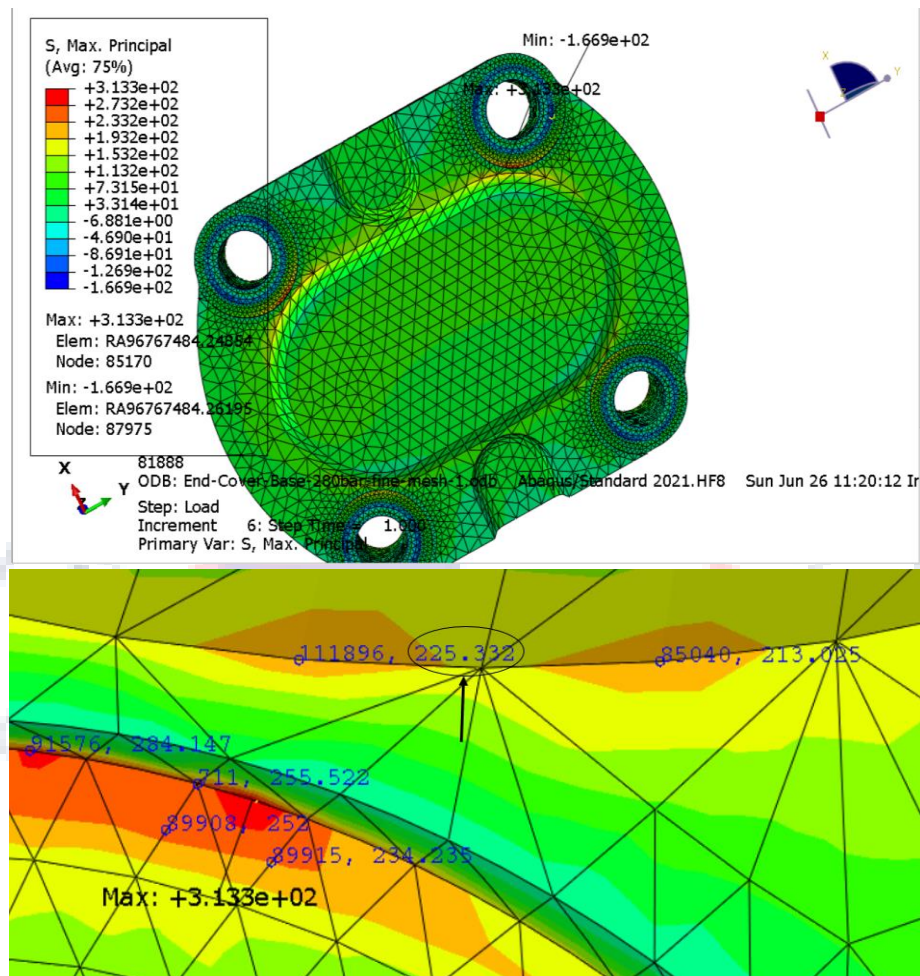


Fig 6. 3: Maximum Principal Stress- Iteration #1

Fig 6.3 shows the maximum principal stress at the joint to be 225.3MPa, which is close to the value obtained from the base model. Generally, for maximum principal stress the value that has to be observed is the one that is at the joint i.e., the region where they end cover is most likely to fail. But a quantitative comparison will show us that the maximum principal stress is higher in other regions due to lack of chamfering.

6.2.2 Deformation

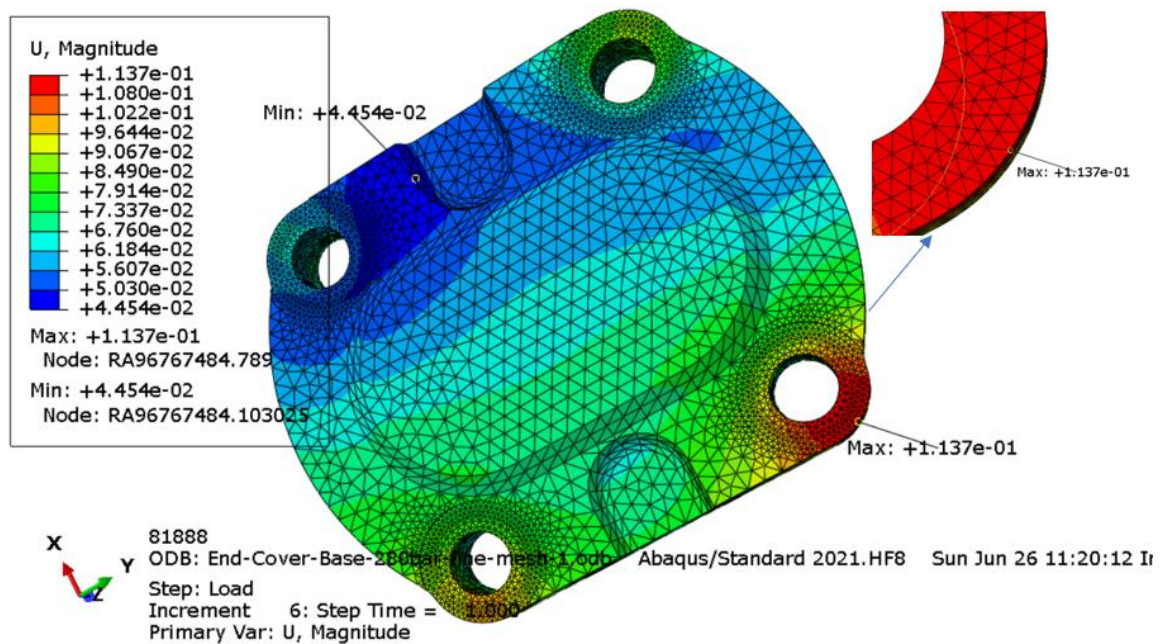


Fig 6. 4: Deformation – Iteration #1

Fig 6.4 shows the deformation for iteration #1 to be 0.1137 mm which is the same as the base model. A similar pattern for deformation is observed in all the other iterations as well i.e., at the suction region of the end cover. A symmetrical deformation value is expected but due to the upward movement of the end cover i.e., sliding, we observe a biased value of deformation.

6.3 Iteration #2 (170466 elements)

Iteration #2 consists of a finer mesh, with the number of elements being increased from 33674 in the base model to 170466 elements. The results are encapsulated as follows-

6.3.1 Maximum Principal Stress

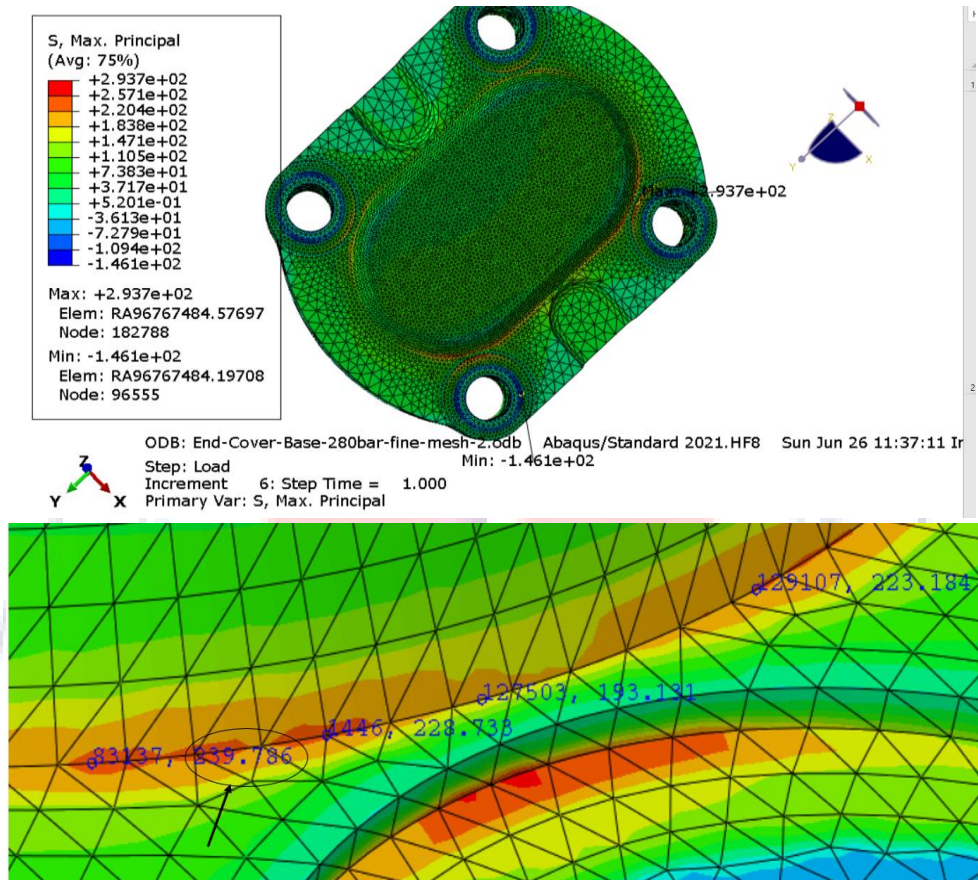


Fig 6. 5: Maximum Principal Stress- Iteration #2

Fig 6.5 shows the maximum principal stress at the joint to be 239.786 MPa, which slightly differs from the value obtained from the base model. The value of maximum principal stress is at the joint that is the critical region where the end cover is most likely to fail, it also shows that the direction of maximum principal stress is perpendicular to the direction of propagation of the crack.

6.4 Iteration #3 (244412 elements)

Iteration #3 consists of a very fine mesh, with the number of elements being increased from 33674 in the base model to 244412 elements. The results are put together as follows-

6.4.1 Maximum Principal Stress

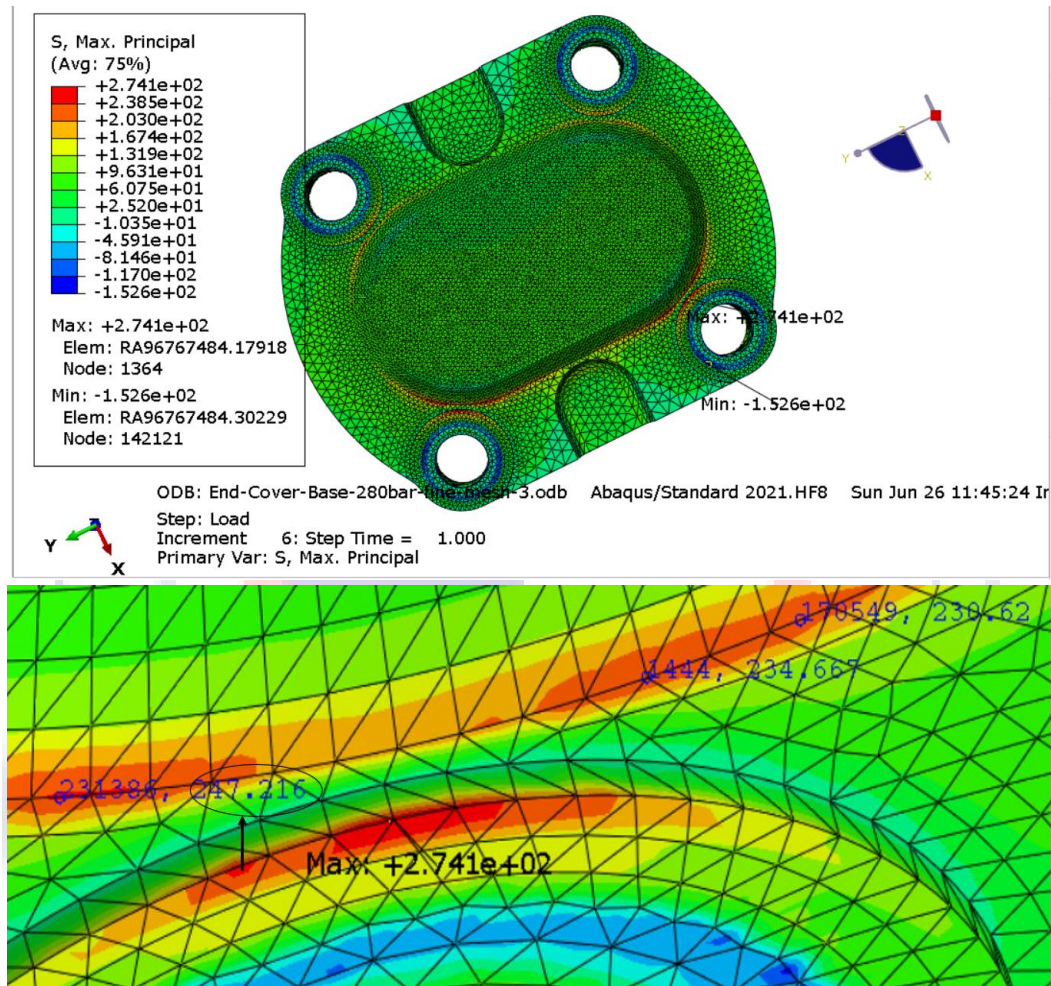


Fig 6. 6: Maximum Principal Stress- Iteration #3

Fig 6.6 shows the maximum principal stress at the joint to be 247.216 MPa, which varies from the value obtained from the base model. This value of maximum principal stress is the one that is most ideal and that matches all the numerical calculations. This design along with iteration #4 is the one that is most likely being shortlisted due to its precise value obtained.

6.5 Iteration #4 (349758 elements)

Iteration #4 consists of a very fine mesh, with the number of elements being increased from 33674 in the base model to 349758 elements. The results are shown as follows-

6.5.1 Maximum Principal Stress

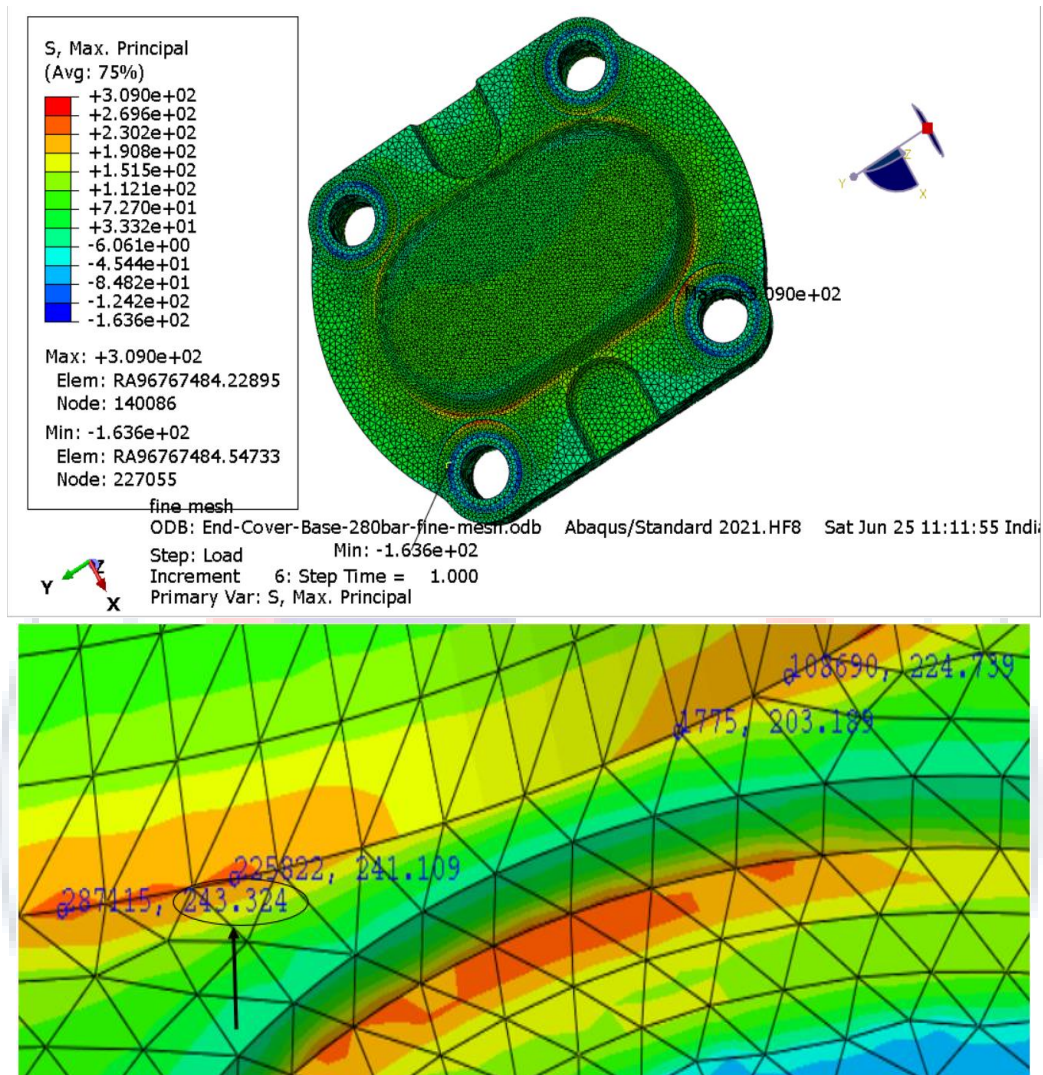


Fig 6. 7: Maximum Principal Stress- Iteration #4

Fig 6.7 shows the maximum principal stress at the joint to be 243.324 MPa, which is close to the value obtained in iteration #3. It is a very fine meshing that has been carried out in this particular iteration and this value is very close to the one in iteration #3. It is the most ideal value and most precise of them. This iteration also proves that the direction of maximum principal stress is perpendicular to the direction of propagation of the crack

6.6 Iteration #5 (576637 elements)

Iteration #1 consists of the finest mesh, with the number of elements being increased from 33674 in the base model to 576637 elements. The results are put together as follows-

6.6.1 Maximum Principal Stress

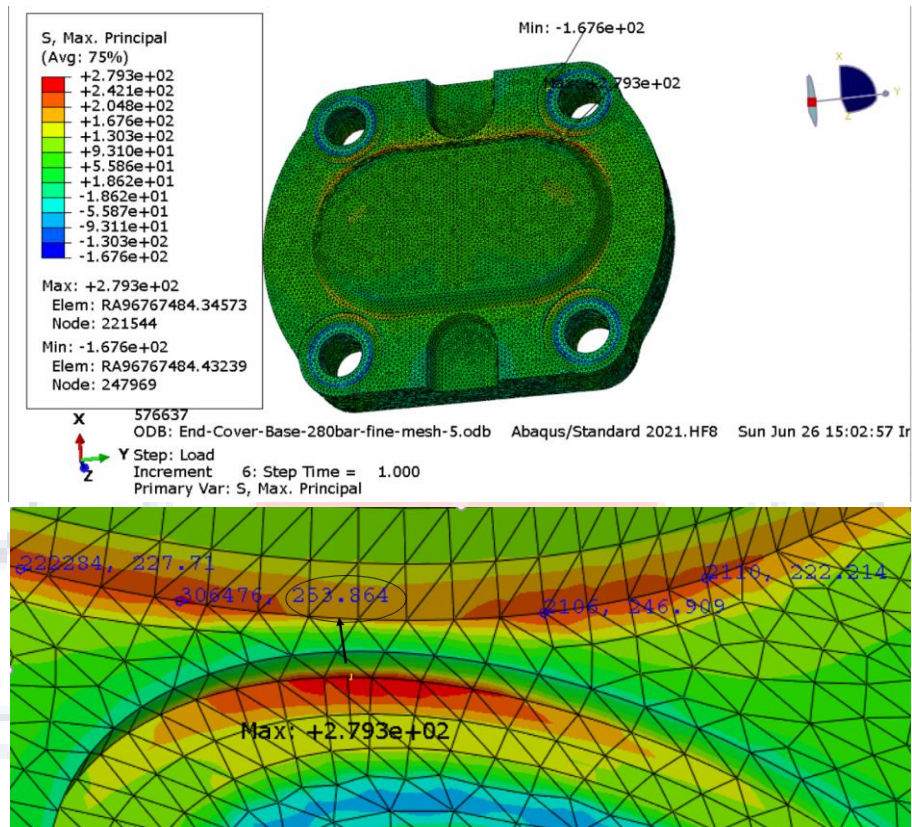


Fig 6. 8: Maximum Principal Stress- Iteration #5

Fig 6.8 shows the maximum principal stress at the joint to be 253.864 MPa, which is slightly close to the value obtained in iteration #3 and iteration #4. In this iteration the finest meshing has been carried out, due to which maximum principal stress is extremely high and thus it can be said that the end cover might fail easily in this case. Hence this particular design was discarded.

Table 6. 1: Summary of results obtained during the iterations

280 bar base model						
Particulars	Base model	Iteration #1	Iteration #2	Iteration #3	Iteration #4	Iteration #5
No. of elements	33674	81888	170466	244412	349758	576637
Maximum Principal Stress at the joint (Mpa)	224.4	225.332	239.7	247.216	243.324	253.864
Maximum Deformation(mm)	0.1137	0.1137	0.1138	0.1138	0.1138	0.1138

Table 6.1 shows that a base model with 33674 elements was analyzed and along with that, 5 iterations were carried out with the number of elements being 81888, 170466, 244412, 349758 and 576637 respectively. The maximum principal stress for the base model was shown to be 224.4 MPa and the maximum principal stresses for the 5 iterations were 225.332MPa, 239.7 MPa, 247.216 MPa, 243.324MPa and 253.864 MPa respectively. It was observed that the maximum deformation for the base model and iteration #1 was 0.1137mm and the maximum deformation for iteration#2, iteration #3, iteration#4 and iteration#5 was 0.1138mm.

CHAPTER 7

CONCLUSION AND FUTURE SCOPE

7.1 Conclusion

In summary, a total of five iterations were carried out for a 280 bar model by varying the mesh sizes and values of maximum principal stress and deformation were observed for all the iterations. These values were compared to the base model and comparisons were made. The following table gives a comparison between all the five iterations.

The following conclusions were made from the results obtained:

- The maximum principal stress is always perpendicular to the direction of the crack
- The values of deformation were observed to be almost the same for all the 5 iterations and thus we can say that these values are permissible.
- The maximum principal stress is similar for iteration #3 and iteration #4 , hence we will take into consideration iteration #4 as a design for future use.
- There is a huge fluctuation in the values of maximum principal stress for iteration #5 and iteration #2. Thus, these iterations will not be considered for future purposes.

7.2 Future Scope

Using the results obtained for these iterations, strains can also be measured using strain gauges and further optimization can be done.

The thickness of the covers can also be varied and different results can be observed. And if favourable, one of the iterations can be implemented for future purposes.

REFERENCES

- [1] Mucchi, E. & D'Elia, Gianluca & Dalpiaz, Giorgio, Simulation of the running in process in external gear pumps and experimental verification. *Meccanica*, vol 47, (721-743), 2018
- [2] Kollek, W. & Warzyńska, Urszula, Energetic efficiency of gear micropumps. *Archives of Civil and Mechanical Engineering*, vol 15, (326-329), 2010
- [3] Fiebig, Wieslaw & Korzyb, M., Vibration and dynamic loads in external gear pumps. *Archives of Civil and Mechanical Engineering*, vol 16, (256-268), 2015
- [4] Osiński, Piotr & Deptuła, Adam & Partyka, M.A. Discrete optimization of a gear pump after tooth root undercutting by means of multi-valued logic trees. *Archives of Civil and Mechanical Engineering*. Vol 13. (422–431), 2013
- [5] Shen, Haidong & Li, Zhiqiang & Lele, Qi & Qiao, Liang. A method for gear fatigue life prediction considering the internal flow field of the gear pump. *Mechanical Systems and Signal Processing*, vol 99. (327-365), 2016
- [6] P. Casoli, A. Vacca, G.L. Berta, Optimization of Relevant Design Parameters of External Gear Pumps, in: *Proc. 7th JFPS Int. Symp. Fluid Power*, Toyama, Japan. vol 3, (112-143), 2008
- [7] Devendran, Ram Sudarsan & Vacca, Andrea. Optimal design of gear pumps for exhaust gas aftertreatment applications. *Simulation Modelling Practice and Theory*. Vol 38. (1–19). 2013
- [8] K Nagamura; K Ikejo, F G Tutulan, “Design and performance of gear pumps with a non-involute tooth profile”, *Proceedings of the Institution of Mechanical Engineers*, 218, B7; *ProQuest Science Journals* vol 2, (689-694), 2001
- [9] Stefanov, Predrag & Savić, Aleksandar & Dobric, Goran. Development and Operational Planning of Power Systems by Comparing Scenarios during Multi-Objective Optimization. *Acta Physica Polonica A* vol 128.

- (132-143), 2015
- [10] Kan, Mehmet & Ipek, Osman & Gürel, Barış. Plate Heat Exchangers as a Compact Design and Optimization of Different Channel Angles. *Acta Physica Polonica A*. vol 128. (1-49) , 2015
- [11] Y.Y. Perng, J. Will, Optimization in ANSYS Work- bench, Ansys INC., 2011.
- [12] L. Alvarez, Ph.D. Thesis, University of Bradford, 2000.
- [13] December 21, 2019 http://pumps.org/Pump_Fundamentals/PD.aspx
- [14] Albert Albers and Eike Sadowski. The Contact and Channel Approach (C&C2-A): Relating a System's Physical Structure to Its Functionality, vol 23, (151–171), 2014
- [15] Albert Albers, Andreas Braun, P John Clarkson, Hans-Georg Enkler and David C. Wynn. Contact and channel modelling to support early design of technical systems, vol 9, (323-342), 2009
- [16] Gerhard Bauer. Ölhydraulik. Grundlagen, Bauelemente, Anwendungen. Springer Fachmedien Wiesbaden, Wiesbaden, vol 32, (170-210), 2016
- [17] Philipp Bergmann and Florian Gruen. Modeling wear of Journal bearings, vol 7, (325-353), 2016
- [18] Bosch Rexroth - KRAMP. December 20, 2019 <https://www.kramp.com/shop-nl/nl/brand/10011/Bosch+Rexroth>.
- [19] Bosch Rexroth AG. Product catalogue. External gear pumps.
- [20] Danfoss. Failure Analysis of Hydraulic Gear Pumps Manual.
- [21] David B. Parker. Positive displacement pumps. Performance and application, vol 15, (87-123), 2018
- [22] Description of a S-N Curve - Fatec Engineering. January 3, 2020
- [23] Gary W.Krutz , Patrick S.K.Chua. Water hydraulics. Theory and applications. Vol 23. (214-223). 2004
- [24] Gear pumps theory. External Gear Pumps, December 21, 2019
-